10216–10229 *Nucleic Acids Research, 2016, Vol. 44, No. 21* *Published online 17 August 2016*
doi: 10.1093/nar/gkw720

Incision of damaged DNA in the presence of an impaired Smc5/6 complex imperils genome stability

Jie Peng and Wenyi Feng*

Department of Biochemistry and Molecular Biology, State University of New York Upstate Medical University, Syracuse, NY 13210, USA

Received February 01, 2016; Revised August 05, 2016; Accepted August 08, 2016

ABSTRACT

The Smc5/6 complex is implicated in homologous recombination-mediated DNA repair during DNA damage or replication stress. Here, we analysed genome-wide replication dynamics in a hypomorphic budding yeast mutant, *smc6-P4*. The overall replication dynamics in the *smc6* mutant is similar to that in the wild-type cells. However, we captured a difference in the replication profile of an early S phase sample in the mutant, prompting the hypothesis that the mutant incorporates ribonucleotides and/or accumulates single-stranded DNA gaps during replication. We tested if inhibiting the ribonucleotide excision repair pathway would exacerbate the *smc6* mutant in response to DNA replication stress. Contrary to our expectation, impairment of ribonucleotide excision repair, as well as virtually all other DNA repair pathways, alleviated *smc6* mutant's hypersensitivity to induced replication stress. We propose that nucleotide incision in the absence of a functional Smc5/6 complex has more disastrous outcomes than the damage *per se*. Our study provides novel perspectives for the role of the Smc5/6 complex during DNA replication.

INTRODUCTION

Eukaryotic DNA replication follows a temporal program where replication origins activate in a staggered order to create a continuum of replication forks progressing through the chromosome before encountering another convergent fork (1,2). Eukaryotic DNA polymerases responsible for processive synthesis have intrinsic nucleotide mis-incorporation of not only mismatched deoxyribonucleoside monophosphates (dNMPs) but also ribonucleoside monophosphates (rNMPs) at a rate of approximately 10^{-7} and 4×10^{-4} (10 000 per 12.5 Mbp of yeast genome), respectively (3–6). Removal of mis-incorporated dNMPs and rNMPs during replication requires concerted actions by distinct protein complexes in the mismatch repair (MMR) and ribonucleotide excision repair (RER) pathways, respectively (7). Virtually all DNA repair pathways require recognition and subsequent excisions of the damaged nucleotide, giving rise to a single-stranded gap in the DNA polymer (7). The mechanisms ensuring such a structural alteration of the chromosome is efficiently repaired and does not lead to further degradation are underexplored. Conceivably, these mechanisms would involve protein complexes directly interacting with the chromosomal DNA and implicated in DNA damage or replication stress response.

One of the three evolutionarily conserved Structure Maintenance of Chromosome (SMC) protein complexes, the Smc5/6 complex, plays a key role in DNA damage repair. The Smc5 and Smc6 proteins, which form the heterodimeric core, together with six other essential Non-SMC Element 1–6 (Nse1-6) constitute the Smc5/6 complex (8–16). Cells with mutations in any subunit of the Smc5/6 complex are hypersensitive to various reagents including hydroxyurea (HU, a ribonucleotide reductase inhibitor), methyl methanesulfonate (MMS, an alkylating reagent) and ultraviolet light (9,12,15–28). Cruciform DNA molecules (X-molecules) representing abnormal recombination intermediates are observed in MMS-treated *smc5/6* mutants (24,29). Removal of recombinogenic proteins such as Rad51, Mph1, Mms2 and Shu1 decreases the level of X-molecules in *smc5/6* cells and rescues their hypersensitivity to replication stress-inducing reagents (24,29,30). Thus, it was established that the key function(s) of the Smc5/6 complex are preventing and/or resolving abnormal recombination intermediates during replication stress. Consistent with this notion loss of a functional Smc5/6 complex can lead to aberrant chromosome segregation during mitosis and meiosis (31–33). Removal of the joint molecule intermediates in meiosis via the XPF-family endonuclease, Mus81-Mms4/Eme1, requires a functional Smc5/6 complex (34,35). Finally, the Smc5/6 complex counteracts replication fork regression (a source of X-molecules) by the Mph1 helicase *in vitro* (36).

On the other hand, studies have also implicated a role of the Smc5/6 complex during an unperturbed S phase (without replication stress). First, transcription of *SMC6* peaks in late-G1 phase and chromosome loading

*To whom correspondence should be addressed. Tel: +1 315 464 8701; Fax: +1 315 464 8750; Email: fengw@upstate.edu

of Smc6 is replication-dependent (33,37–39). Second, impaired Smc5/6 function (via temperature-sensitive mutations) in S phase, but not in G2 phase, resulted in anaphase bridges and mitotic failure (33). More recent studies also suggest related replicative roles of the Smc5/6 complex in promoting replication fork progression through ribosomal DNA tandem repeats or in extraneous topological stress (40,41). However, the precise function(s) of the Smc5/6 complex in S phase are still unclear, at least in part owing to the lack of replication studies of the *smc5/6* mutants in the absence of replication stress. A recent study employed a creative approach to deplete cells of the Smc5/6 complex during S phase using cell cycle-specific promoter and observed minimal impact on S phase progression (42). Instead, it argued for an essential role of the Smc5/6 complex in regulating sister chromatids separation during G2. Nevertheless, it stands to reason that the absence of a protein might have fundamentally different cellular impact than a defective protein due to mutations.

We set out to analyse the replication dynamics in a hypomorphic budding yeast mutant, *smc6-P4,* which carries a K239R mutation near the ATPase domain of Smc6p (24). Our results also revealed minimal changes in the S phase dynamics in the *smc6* mutant. However, we did observe an early S phase-specific phenotype that was best explained by the presence of ribonucleotide and/or single-stranded DNA (ssDNA) gaps in the replicated DNA of *smc6* cells. We demonstrated that *smc6-P4* cells accumulated rNMPs and contained higher level of ssDNA than WT cells. We also observed that during replication stress by HU *smc6* cells showed more extensive fork progression than WT. These data are consistent with a function of the Smc5/6 complex in restraining replication fork movement and preventing nucleotide mis-incorporation. We tested if inhibiting DNA repair would exacerbate the *smc6* mutation by examining the genetic interactions between *smc6-P4* and deletion mutations of key enzymes in the RER and MMR pathways. Unexpectedly, inactivation of nuclease functions in either pathway alleviated, rather than exacerbated, the hypersensitivity to replication stress of the *smc6* mutant. In addition, removal of nucleases in base excision repair (BER) and nucleotide excision repair (NER) inducible by DNA alkylation damage similarly rescued drug sensitivity of the *smc6* mutant. Therefore, we concluded that initiating DNA repair in the *smc6* mutant during replication stress is detrimental to cell viability. We also suggest a protective role of the Smc5/6 complex of DNA repair intermediates following the initial damage incision. Our study thus provides a novel view of the Smc5/6 complex function at the crossroads of DNA transactions.

MATERIALS AND METHODS

Yeast strains and cell growth

Yeast strains used in this study are listed in Supplementary Table S3. They are derived from A4070, a *RAD5* derivative of W303 (*MAT**a*** or ***α*** *ade2-1 can1-100 ura3-1 his3-11,15 leu2-3,112 trp1-1 rad5-535*) (43) or the EUROSCARF collection of nonessential yeast deletion mutants (*MAT**a*** *ura3Δ leu2Δ his3Δ met15Δ YFGΔ::KAN*) (44) or Δ/(-2)/-7B-YUNI300 (*MAT**a*** *CAN1 his7-2 leu2Δ::KanMX ura3Δ trp1-289 ade2-1 lys2-ΔGG2899-2900 agp1::URA3-OR2*) (45). Cells were grown in YPD medium at 25°C unless otherwise noted. Double mutants, unless otherwise noted below, were constructed using standard mating, zygote selection, followed by tetrad dissection. To generate *smc6-P4 hnt3Δ*, the endogenous *HNT3* was replaced by a *KAN* cassette by gene replacement in the *smc6-P4/SMC6* diploid cells followed by tetrad dissection. The *KAN* cassette was generated by polymerase chain reaction (PCR) on genomic template DNA from the *hnt3Δ* strain from the EUROSCARF collection using the following primers: HNT3_L, 5′-gtcgaattcTGACGGATGAAGAGCTGAGAG-3′ and HNT3_R, 5′-ccgaagcttCCCATAAGAGATGACCGTGATC-3′. During the construction of *smc6-P4 pol2* double mutants, it was necessary to distinguish *pol2-M644L* from *pol2-M644G* mutation and *SMC6* from *smc6-P4* by PCR and sequencing. The following primers were used to amplify the *SMC6* and *POL2* loci, respectively: SMC6_L, 5′-TGCGGTCAAGGATTATTGCG-3′, SMC6_R, 5′-CCATGTCCATCGCTGTTCAG-3′; and POL2_644_L, 5′-ATCCGAGACTTACGTGGGTG-3′, POL2_644_R, 5′-GAAGCCGGATTGTGCCTAAG_3′.

Spot assay

Single colony from each yeast strain under analysis was inoculated in 5 ml of YPD medium and the culture grown overnight at 30°C. The resulting culture was then used to inoculate 25 ml fresh YPD medium. When the culture reached late log phase (OD_{600} ∼1.0), cell pellet was collected by centrifugation, washed in 10 ml of '-N' medium (1.61 g/l YNB without $(NH_4)_2SO_4$ or amino acids, 94 mM succinic acid and 167 mM NaOH) and re-suspended in 1 ml of '-N' medium. Cells were then sonicated in a Bioruptor (Diagenode) to reduce clumping before measuring cell concentration by a hemocytometer. Cells were first diluted to 10^7 cells per ml followed by 1:10 serial dilutions. Two microlitres of each serial diluted culture was spotted onto solid YPD medium or that containing 10 mM HU or 0.015% MMS unless otherwise noted and the plates were incubated at 30°C. Plates were photographed every 24 h for 2–3 days.

Flow cytometry

One millilitre of cells collected in the density transfer experiment were spun at 5000 rpm for 5 min and the pellet was washed with autoclaved glass-distilled (AGD) H_2O and resuspended in 1 ml of cold 70% ethanol. The ethanol-fixed samples could be stored at 4°C. A total of 500 μl of fixed cells were used for flow cytometry analysis. The cell pellet was first washed by 1 ml of 50 mM sodium citrate, pH 7.4, then resuspended in 1 ml of 50 mM sodium citrate, pH 7.4 with 50 μg/ml RNase A and incubated at 50°C for 1 h. Fifty microlitres of 20 mg/ml protein kinase K was then added to the cells and continue incubation at 50°C for another hour. The cells were then spun and resuspended in 1 ml of 50 mM sodium citrate, pH 7.4 with 1 μM of Sytox Green (Life Technologies) at 4°C overnight in the dark. Following brief sonication using a Bioruptor to reduce clumping, 10 000 cells from each sample were analysed on a Becton

Dickinson Fortessa Cell Analyser (BD Biosciences). Data were analysed by FlowJo.

Density transfer coupled with microarray analysis

Detailed procedures for density transfer, slot blotting, microarray hybridization and data analysis were described previously (46). Briefly, cells were grown in '-N' medium supplemented with 0.1% D-Glucose-$^{13}C_6$ (Sigma 389374-2G), 0.01% Ammonium-$^{15}N_2$-sulfate (Sigma 299286-1G) and required amino acids at 25°C for at least 8 generations. A total of 200 nM α-factor was added to synchronize cells until fewer than 10% budded cells remained in the culture. Cells were filtered and transferred to normal Y-complete medium containing 200 nM α-factor for acclimation for 30 min, followed by the addition of 0.02–0.03 mg/ml pronase to degrade α-factor and cell cycle release into S phase. Samples were collected every 10 min for either flow cytometry or genomic DNA isolation. Genomic DNA was extracted and digested with *Eco*RI restriction enzyme. The digested DNA was loaded onto CsCl gradient for ultracentrifugation and followed by fractionation. An aliquot of each fraction was used for slot blot analysis and the remainder used for microarray hybridization. Slot blotting using a genomic DNA probe was used to determine the fractions containing HH and HL DNAs. The respective fractions were then pooled and the differentially Cy5- or Cy3-dUTP-labeled HH and HL DNAs were co-hybridized onto Agilent Yeast Whole Genome ChIP-on-Chip 4 × 44K (G4493A) microarrays following the manufacturer's instructions and the features were scanned by an Agilent G2565B scanner and the data extracted by the Agilent Feature Extraction software (v9.5.1). Raw microarray data were Lowess smoothed over a 36 kb-window and percentage of replication (% Rep) was calculated for each genomic locus, followed by normalization using the maximum % Rep obtained from slot blot analysis as described (46). DNA fragments containing ARS607 or ARS609 were amplified by PCR from the yeast genome with the following primers and used for Southern blot: ARS607-F, 5′-CGATGTCCGCATCACTGGCA-3′; ARS607-R, 5′-CAGGTGAATCAGAATGGCTC-3′; ARS609-C, 5′-GCTGATTGTGTAATAGTGGTG-3′; ARS609-D, 5′-CATTGTACTAGGATGTTTCGC-3′.

Quantification of total level of ssDNA

Three hundred millilitres of exponentially growing cells (~10^7 cells/ml) were incubated for 3 h in the absence or presence of 10 mM HU before harvesting for DNA preparation. Genomic DNA was isolated according to the 'NIB-n-grab' method (http://fangman-brewer.genetics.washington.edu/nib-n-grab.html). Slot blot analysis of bulk level ssDNA was performed similarly as described (47). Briefly, un-denatured (native) genomic DNA was slot blotted in triplicates, 1 μg per slot, onto nylon membranes. An additional 100 ng of each genomic DNA sample was heat-denatured in 0.2 N NaOH and also slot blotted in triplicates, serving as a total DNA control. The membranes were hybridized with a genomic DNA probe and signal quantification was done with ImageJ. Total % ssDNA was calculated as $\text{Signal}^{\text{Native}}/(10 \times \text{Signal}^{\text{Denatured}}) \times 100$. Reported values were averaged from four independent experiments. The *ARS1* fragment was amplified from the yeast genome with the following primers: ARS1-F, 5′-GGAGGGAGATGGATTGTTGA-3′; ARS1-R, 5′-GGAGGCAAGTGCACAAACAA-3′.

Genomic ssDNA mapping by microarrays

Detailed procedures for ssDNA labeling, microarray hybridization and data analysis were described previously (48). Briefly, cell cultures were grown and cell cycle synchronized similarly as in density transfer except that normal YPD medium was used. G1 control sample was collected prior to cell cycle release and the S phase sample was collected 1 h after pronase addition. Cell pellets were washed with 50 mM EDTA, pH 8.0 before casting into 0.5% low melting agarose gel plugs in 50 mM EDTA, pH 8.0. The embedded cells were then spheroplasted in-gel and the resulting chromosomal DNA were labelled for ssDNA at 37°C for 3 h. The DNA was eluted from the plugs by either electrophoresis in dialysis tubing with a molecular weight cut-off of 12–14 000 (Spectrum Laboratories, Inc) in 0.5x TBE at 3V/cm for 4 h or by β-agarase (New England Biolab) digestion. The eluted DNA was then sonicated by Bioruptor and purified using the QIAquick PCR Purification Kit. Differentially Cy5- or Cy3-dUTP-labelled G1 and S phase DNA were co-hybridized onto microarrays and feature extracted similarly as described above. Raw data were Lowess smoothed over a 6 kb window and subsequent data analysis was performed as previously described (48).

Definition of early and late origins in the W303 strain background

Rad53 check- and unchecked-origins were previously defined as those origins that are subject to (Rad53-checked, or inferred late origins) or exempt from (Rad53-unchecked, or inferred early origins) the replication checkpoint control in the RM14-3a strain background (47). We performed ssDNA mapping in isogenic WT and *rad53K227A* strains in the W303 background and curated origins activated in the W303 background. We then compared these origins to 626 confirmed or likely origins from the OriDB (http://oridb.org, v2.0.1) and those origins that have corresponding entries in OriDB were selected for a final list of 467 W303-specific origins (205 early origins and 262 late origins, to be described elsewhere).

Meta-analysis of %Rep in DT experiments and origin-associated ssDNA

Meta-analysis of microarray data (%Rep or relative ratio of ssDNA) was performed similarly as described (49). Lowess smoothed values of either %Rep or ssDNA ratio with a 250-bp step window were used for calculating the average level of signals in a 20-kb window on both sides of the origins. For the DT experiments the analysis was performed for both early and late origins. The maximal level of %Rep in the 40 kb window of the two groups of origins were then plotted against the genomic average %Rep for each sample in the three DT experiments. For measuring fork distance

from the ssDNA profiles only the 205 early origins were used as HU precluded the majority of late origins from firing. The maximal ssDNA value in the 20-kb window on the left and right of the origin were determined as Max_L and Max_R, respectively, in each experiment. Likewise, the minimal ssDNA values were determined as Min_L and Min_R in each experiment. The position at which the average value between Max and Min occurred in the left and right window was converted to distance (for origin position was set arbitrarily at 0) as $Dist_L$ and $Dist_R$, respectively. The replication fork distance ($Dist_{ave}$) was calculated as the average of $Dist_L$ and $Dist_R$, respectively, from each experiment. The final replication fork distance was averaged from multiple biological replicate experiments. Total amount of origin-associated ssDNA was determined by integrating the area under the curves above the average value of Min_L and Min_R for WT and *smc6*, respectively. For measuring origin activation from the ssDNA profiles all 467 W303-specific origins were analysed. A 5-kb window on both sides of the origins was used instead of the 20-kb window to better differentiate ssDNA associated with close-spaced origins. Sub-telomeric origins and origins with poor sequence coverage (<5% in the chosen window on either side of the origin) were also excluded from the analysis. The maximal ssDNA value in the 5-kb window flanking each origin was similarly determined as above. Origins with both Max_L and Max_R being at least three standard deviations above the genomic median were defined as activated in each experiment, but only origins that showed activation in at least two independent experiments were considered activated in the final call.

RESULTS

Comparative analysis of replication dynamics genome-wide

We studied the replication dynamics in the *smc6-P4* mutant and an isogenic WT using a previously described method of density transfer (DT) coupled with microarray (2,46). Briefly as outlined (Figure 1A), we synchronously released cells that were cultured in medium containing heavy isotopes from G1 into S phase in fresh medium containing light isotopes. Thus, replicating DNA would adopt a hybrid density (HL, for 'heavy-light') compared to a uniform density (HH, for 'heavy-heavy') of the unreplicated DNA, which can be separated from each other in a cesium chloride (CsCl) gradient using ultracentrifugation. We collected samples every 10 min up to 120 min after the G1/S transition in three independent DT experiments (DT1-3). We then calculated the percentage of replication (%Rep) for a specific DNA fragment or average genomic DNA in each sample by slot blot analysis. The observed %Rep values were then normalized to account for non-cycling cells in each culture.

Both WT and *smc6* cells synchronously entered the cell cycle, though there appeared to be an advanced entry into S phase in the *smc6* cells compared to WT (Figure 1B). However, the ∼10–20% budded cells at the G1/S transition most likely represent non-cycling cells. Flow cytometric profiles showed that the *smc6* mutant progressed through S phase faster than WT cells (Figure 1C). Consistently, we detected more advanced replication timing of the genomic DNA in the mutant, as exemplified by an average T_{Rep} (the elapsed time after release from G1 when half of the maximal replication level is achieved) of 47.7 min compared to 52.8 min for WT from three DT experiments (Figure 1A and D and Supplementary Table S1). We then analysed the genomic replication profile for each of the samples collected between 30 and 60 min (Figure 1A and Supplementary Table S2). Because *smc6* cells always showed advanced replication timing to WT in the same experiment it was difficult to compare their replication profiles at the same time point during S phase (Figure 2A and Supplementary Figure S1). To circumvent this problem we compared samples from different DT experiments with similar level of genomic DNA replication. To do so, we first performed a meta-analysis (49) of %Rep across a 40 kb region over each of the early and late origins in the genome (details of definition in Materials and Methods). We then compared samples both within and between WT and *smc6* strains if they shared similar %Rep values. The majority of such comparisons revealed similar replication profiles between WT and *smc6* cells (not shown) except for early S phase samples, i.e. between WT at 30 min from DT1 (10.3%) or WT at 35 min from DT3 (11.1%), and *smc6* at 30 min from DT2 (10.8%) (Figure 2B and Supplementary Table S2). The *smc6* mutant showed relatively higher %Rep surrounding the early origins than WT, accompanied by a lower %Rep at the summits of the origins in the mutant (Figure 2B). No such difference was observed for the late origins among these samples, or any other samples sharing similar %Rep (data not shown). These results suggested that the replication dynamics in the *smc6* mutant deviated from that of the WT, at least at the early origins. We then asked if replication at the origins differ from genome average throughout S phase. To do so we assembled a virtual replication progression for WT and *smc6* cells by using samples that contained variable level of %Rep from the three experiments. We plotted the maximal %Rep over the 40 kb region across all early or late origins against the genomic %Rep in the same sample. Both the early and late origins showed steady progression proportional to the genomic average over time (Figure 2C and D), indicating that the phenotype we observed for samples in early S phase was likely transient and did not impact overall replication progression.

This early origin-specific phenotype can be explained by two non-mutually exclusive causes. First, the *smc6* cells presented lower synchrony than WT while entering S phase. Second, the replication forks descended from the early origins progressed faster in the *smc6* mutant at the early stage of S phase, but the replicated (HL) DNA behind the forks suffered from some unknown defects that resulted in its apparently lower quantity. We hypothesized that HL DNA at the early origins in the mutant possessed higher density than the normal hybrid density, causing it to sediment closer to the HH DNA. Thus, when the HH and HL fractions were pooled for microarray hybridization, the HL DNA fragments from early origins would be under-represented whereas the HH DNA would be over-represented, hence lower %Rep than the actual level. We tested this hypothesis by slot blot analysis of DNA fragments containing either an early (*ARS607*) or a late (*ARS609*) origin (Figure 3A). The *ARS607* profiles showed that the HL DNA in the mutant sedimented relatively lower (closer to the bottom of the

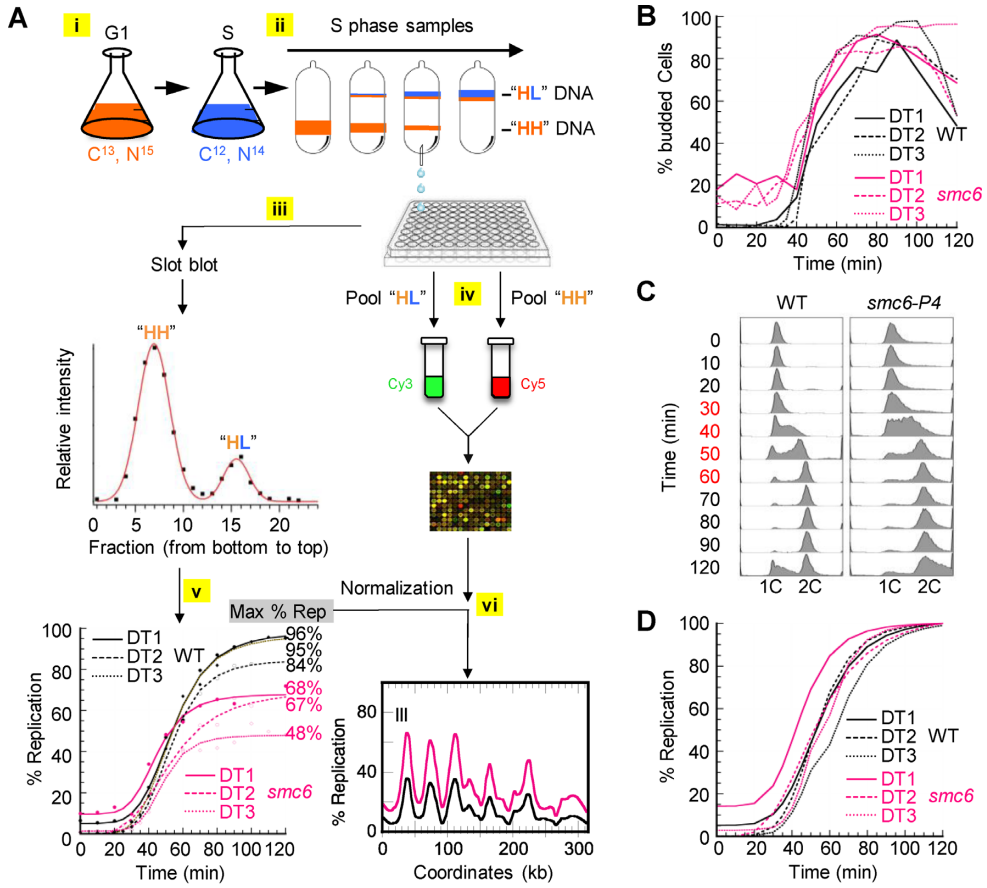

Figure 1. S phase progression is accelerated in the *smc6-P4* mutant under unchallenged condition. (**A**) Schematic representation of density shift experiment: (**i**) sample collection from cells that were cultured in medium containing heavy isotopes (^{13}C-glucose and ^{15}N-ammonium sulfate) synchronously released from G1 into S phase in fresh medium containing light isotopes (^{12}C-glucose and ^{14}N-ammonium sulfate), (**ii**) separation of replicated (HL, 'heavy/light') DNA and unreplicated (HH, 'heavy/heavy') DNA on CsCl density gradient, (**iii**) fractionation of the gradient for slot blot analysis and (**iv**) differential labelling and microarray co-hybridization of pooled HL and pooled HH DNA from the gradient. Slot blot facilitates (**v**) replication kinetic analysis to derive maximal percentage of genomic DNA replication subsequently used for (**vi**) normalizing microarray data and construction of replication profiles for comparisons between samples. (**B**) Budding indices indicate similar kinetics of cell cycle entry in the *smc6-P4* and the WT cells in three independent DT experiments. (**C**) FACS profiles (number of cells plotted against contents of genomic DNA) of the *smc6-P4* mutant and the WT cells from DT1 at indicated times following cell cycle release from G1/S transition ('0'). '1C' and '2C' denote positions of genomic DNA before and after replication. (**D**) Genomic replication kinetics of the *smc6-P4* and WT cells in each experiment. Maximal normalized % of genomic DNA replication in each sample is as indicated.

tube) than that in the WT, whereas the *ARS609* profiles were similar between the WT and mutant, consistent with our hypothesis (Figure 3B). Ribonucleotides and ssDNA gaps in duplex DNA can both increase its buoyant density (50,51), and incision of rNMPs from the DNA produces ssDNA intermediates. Therefore, we wondered if the *smc6* mutant incorporates rNMPs at a higher rate. If so, removal of RNase H2 would be detrimental to the *smc6* mutant.

Removal of RNase H2 *alleviates* the sensitivity to replication stress of the *smc6-P4* mutant

The RER pathway is initiated when RNase H2 incises the 5′-side of the rNMP, but complete removal of the rNMP occurs after the incision of its 3′-side by the Fen1/Rad27 nuclease (52). Topoisomerase I can also incise the rNMP in DNA, albeit less frequently than RNase H2 (53). Deletion of the gene encoding the catalytic subunit of RNase H2, *RNH201*, despite having no impact on the growth of *smc6* cells without replication stress, actually rescued the HU and MMS sensitivity of the mutant (Figure 4A). We confirmed this observation as well as established the specificity of this genetic suppression as follows. First, removal of one of the two regulatory subunits, Rnh203 (54), also rescued drug sensitivities of the *smc6* mutant (Figure 4B). Second, removal of RNase H1, which functions primarily in resolving RNA:DNA hybrids with tandem rNMPs as in transcriptional R-loops (55), did not suppress *smc6-P4* (Figure 4C). Third, a 'separation-of-function' mutant of *rnh201* that is defective in rNMP removal in the RER pathway but not in processing R-loops, *rnh201-P45D-Y219A* (56), also rescued the drug sensitivities of the *smc6* cells (Figure 4D). Finally, removing the Rad27/Fen1 nuclease also suppressed the drug sensitivity of the *smc6* mutant (Figure 4E). Therefore, we propose that (i) the *smc6* mutant accumulates substrates for the RER pathway through rNMP incorporation during replication and not co-transcriptional R-loop formation; (ii) the incision and possibly subsequent processing

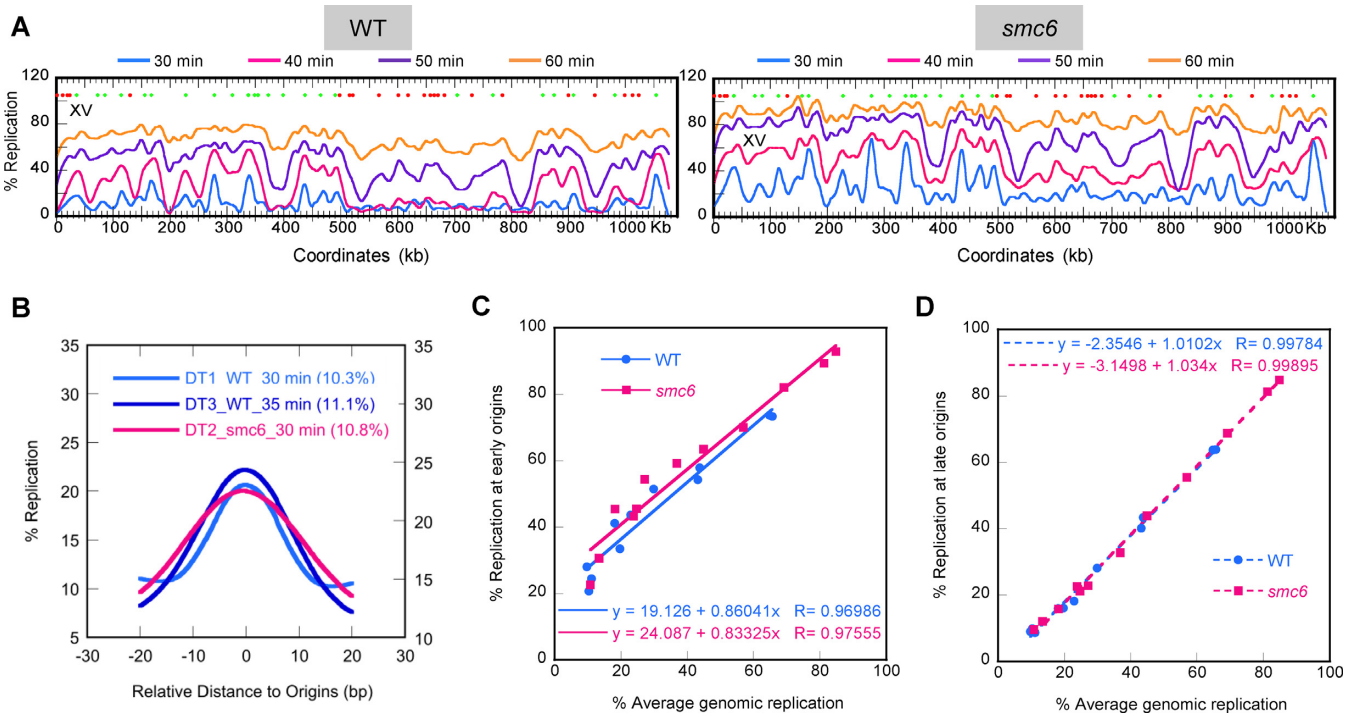

Figure 2. Genome-wide replication dynamics show *smc6-P4* cells with advanced average replication timing to WT. (**A**) Overlay of replication profiles with normalized %Rep plotted against chromosome coordinates (kb) for ChrXV, for all samples analysed by microarray in the DT1 experiment. Please see Supplementary Figure S1 for all three DT experiments. Origin locations derived from OriDB are shown: 205 early origins (solid green diamonds) and 262 late origins (solid red circles) (see Materials and Methods for details). (**B**) Meta-analysis of %Rep over early origins in the early S phase samples which share similar genomic average %Rep between WT and *smc6* cells. (**C**) Comparison of %Rep of early origins (determined as the maximal %Rep in the meta-analysis profile for each sample) with %Rep of genomic average. (**D**) Same as in (C), for late origins.

of rNMPs are detrimental to the *smc6* mutant. We further demonstrated that inactivating RER conferred the suppression of drug sensitivity of the *smc6* mutant by specifically inactivating RNase H2, and not Top1, consistent with a minor role of the latter in the RER pathway in the presence of a functional RNase H2 (Figure 4F).

Genetic suppression by *rnh201Δ* is specific for the *smc6* mutation

The *smc6* mutant is among a group of mutants including *esc2Δ* and *sgs1Δ* that are known to accumulate recombination intermediates (24). It has been shown that removing recombination-promoting proteins such as Mph1, Mms2 and Shu1 synthetically rescues the MMS sensitivity of *smc6-P4*, *esc2Δ* and *sgs1Δ* mutants (24,29). Thus, if RNase H2 also functions as a recombinogenic protein, its removal would also benefit the *esc2Δ* and *sgs1Δ* mutants. However, we did not find synthetic interaction between *rnh201Δ* and *esc2Δ* (Supplementary Figure S2A). In fact, *rnh201Δ* showed synthetic sickness with *sgs1Δ* (Supplementary Figure S2B), as previously shown (56–59). This result suggested that RNase H2 does not function as a recombinogenic protein and that its removal does not prevent the formation of recombination structures in mutants other than *smc6*. Because Smc6 physically interacts with Rtt107 during DSB repair (60,61) we also tested for but did not observe a genetic suppression of *rtt107Δ* by *rnh201Δ* (Supplementary Figure S2C). This result suggested that Smc6 has a distinct function during replication stress-induced RER, which is independent of Rtt107. Finally, we also checked if *rnh201Δ* could suppress other mutations in the Smc5/6 complex, such as *smc6-56* and the *mms21-11* mutation in the SUMO ligase Mms21 (62,63). As shown in Supplementary Figure S2D and E, *rnh201Δ* rescued *smc6-56* but not *mms21-11*, suggesting that the genetic suppression by *rnh201Δ* is allele-specific.

The *smc6* mutant accumulates rNMPs and ssDNA

We then tested if the *smc6* mutant incorporates rNMPs at a higher rate than normal by alkaline gel electrophoresis of genomic DNA. Incorporated rNMPs was subject to base catalysis of the 2′-OH group and subsequent breakage of the phosphodiester bond, thus giving rise to smaller DNA fragments upon strand separation (64). We only compared the genomic DNA from exponentially growing cell cultures without HU treatment for the following reason. We rationalized that the HU treatment (for 2–3 h), by partially synchronizing the cell cycle in early S phase, enriched for nascent DNA fragments varying in size due to differential replication fork speed among different strains. Thus, without further correcting the intrinsic size difference of the template DNA it is difficult to compare HU-treated samples at the present. In the absence of HU *rnh201Δ* cells exhibited enrichment of smaller DNA fragments (Figure 5A and B), as previously described (4,5). The *smc6* mutant also showed increased level of small DNA fragments, though to a lesser

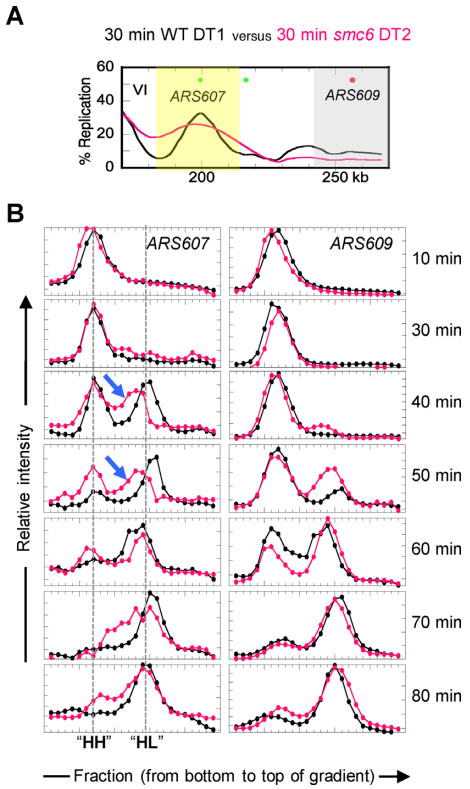

Figure 3. Replicated (HL) DNA in the *smc6* mutant shows relative higher density than that in the WT. (**A**) Selected origins at higher resolution showing relatively lower amount of replicated DNA at *ARS607* (shaded yellow) compared to the flanking regions in the *smc6* mutant. WT cells show expected patterns where replicated DNA is the highest at the center of these early origins. (**B**) Slot blot analysis confirms HL DNA in the mutant at *ARS607* sediments lower on the CsCl gradient, hence possessing a higher density, than that in WT. *ARS609*, a late origin (shaded grey in (A)), served as control.

extent than the *rnh201* mutant (Figure 5A and B). Finally, the *smc6 rnh201* double mutant showed a distribution of DNA fragments between those of the *rnh201* and *smc6* single mutants (Figure 5A and B). These observations indicated that the *smc6* mutant indeed accumulated more rNMPs than WT cells. Moreover, they also suggested that incision of rNMPs from the *smc6* cells did not lead to complete repair as there was merely marginal difference between the base catalysis-induced strand breakage in *smc6* and *smc6 rnh201* cells.

We then asked if the incision of rNMPs leaves ssDNA gaps, which could in turn produce toxic homologous recombination intermediates. To do so, we directly measured ssDNA level by slot blotting undenatured genomic DNA followed by hybridization with a genomic DNA probe, as previously described (65). Our results demonstrated that *smc6* cells indeed accumulated more ssDNA than WT, but only specifically during HU treatment (Figure 5C). Moreover, the ssDNA level in *smc6* cells was reduced by the *rnh201Δ* mutation (Figure 5C). It is also noteworthy that the ssDNA levels in cells exposed to HU were not significantly different from untreated cells, likely due to the low level of replication stress by transient exposure (3 h), as opposed to several days in the spot assay, to 10 mM HU. Nevertheless, consistent with our hypothesis removal of RNase H2 activity reduced the level of ssDNA in the *smc6* mutant in HU (Figure 5C).

smc6 cells does not accumulate a toxic adenylate monophosphate intermediate

Our results thus far supported the hypothesis that incision of damaged DNA in the *smc6* mutant is detrimental to cell survival during replication stress. We then asked if toxic intermediates following rNMP incision constitute the reason for the demise of the *smc6* mutant. The RER pathway can be blighted by either abortive ligation of the incised rNMP to an adenylate monophosphate (AMP, transferred from a DNA ligase I-AMP intermediate after ATP hydrolysis) and formation of a toxic 5′-adenylated (5′-AMP) RNA–DNA adduct (66) or by Top1-mediated formation of a toxic 2′-3′ cyclic phosphate intermediate in the DNA (53,67–68). Removal of the 5′-AMP requires Hnt3, a functional homolog of the mammalian enzyme, Aprataxin (66,69). Therefore, if the incision of rNMPs in the *smc6* mutant led to abortive ligation and 5′-AMP formation, deleting *HNT3* would be detrimental. We did not observe any synthetic sick or lethal interactions between *smc6-P4* and *hnt3Δ* (Supplementary Figure S2F). Therefore, we concluded that the toxic intermediate following rNMP incision in the *smc6* mutant is unlikely to be a 5′-AMP-modified DNA:RNA hybrid. The lack of interaction between *smc6* and *top1Δ* (Figure 4F) also precludes the conclusion that cyclic phosphate intermediates formed in the *smc6* mutant.

The *smc6-P4* mutant shows unrestrained fork progression during acute exposure to HU in S phase

Our analysis so far suggests that the *smc6* mutant suffers from rNMP incision during replication stress, possibly because it leads to unsupervised ssDNA formation that ultimately generates toxic replication intermediates. It is unclear how these defects relate to a potential role of the Smc5/6 complex in regulating replication fork progression. To more rigorously test if replication fork progression is defective in the *smc6* mutant, we analysed replication fork-associated ssDNA genome-wide in WT and *smc6* cells using a previously described ssDNA mapping method (47,48). We detected significant levels of ssDNA at early but not late origins, suggesting that the S phase checkpoint was active in both WT and *smc6* cells during HU treatment (Figure 6A). The ssDNA signals at many of the origins formed 'split peaks' in the WT cells, indicative of well-resolved bidirectional replication forks. In contrast, the ssDNA signals appeared broader and noisier in the *smc6* mutant, suggesting that replication forks had traversed a greater distance and left more ssDNA behind (Figure 6A). To measure average replication fork distances we used a meta-analysis to quantify ssDNA encompassing a 40 kb region centering on 205 early origins, the predominant group of activated origins in *smc6* cells, in three independent experiments (Figure 6B). We calculated that replication forks traversed ∼1.6-fold the distance in the *smc6* mutant (7167 bp) of that in WT (4542 bp) ($P = 0.02$, Student's *t*-test) (Figure 6C). These data support the notion that Smc5/6 plays a role in restraining replication fork progression. However, we acknowledge

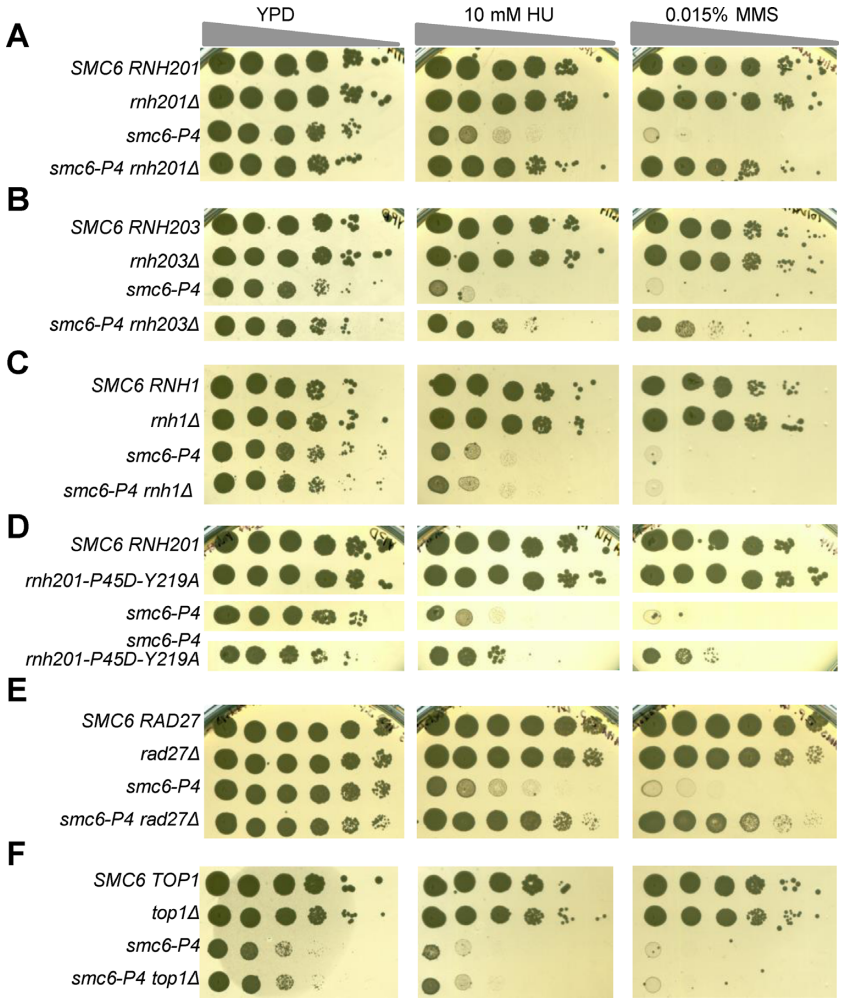

Figure 4. Inactivation of the RER pathway specifically rescues hypersensitivity to replication stress by the *smc6-P4* mutant. Late log phase cultures of the indicated cells were 1:10 serial diluted (1:5 for panel E) and 2 μl of the cells from each dilution was spotted on either YPD plates or YPD plates containing 10 mM HU or 0.015% MMS. Note 0.005% MMS was used for the analysis with *rad27Δ,* which renders cells hypersensitive to 0.015% MMS. (**A**–**B**) Lack of catalytic subunit Rnh201 (A) or one of the regulatory subunit Rnh203 (B) of RNase H2 rescues the drug hypersensitivity of the *smc6-P4* mutant. (**C**) Removing RNase H1 does not affect the drug hypersensitivity of the *smc6* mutant. (**D**) Inactivation of the single rNMP processing function with intact R-loop processing function of RNase H2 suppresses the *smc6* mutant. (**E**) Removal of flap endonuclease, Rad27/Fen1, rescues the drug hypersensitivity of the *smc6* mutant. (**F**) Loss of Top1 does not suppress *smc6.*

that equating the HU-induced ssDNA track length to replication fork distance is contentious *a priori*. For instance, it may be argued that ssDNA is a by-product during homologous recombination and does not reflect fork progression *per se*. For instance it was demonstrated that an Smc5/6 complex mutant, *nse5-ts1*, showed very different BrdU IP-on-chip profile from WT (70). Therefore, we asked if removing the recombinase Mph1 from *smc6* cells has any impact on the ssDNA track distance. If indeed ssDNA formation were merely the result of recombination, we would expect that the *smc6 mph1Δ* double mutant to show a shorter ssDNA track in the meta-analysis. Our data indicated that there was no significant difference between the ssDNA track lengths between *smc6* and *smc6 mph1Δ* cells (Figure 6D and E). This result underscores the validity of inferring fork distance using ssDNA mapping. We then tested if RNase H2 impacts replication fork progression in the *smc6* mutant. Interestingly, *rnh201Δ* cells showed longer fork distance than WT and similar distance as *smc6* cells (Figure 6D and E). This result suggests that impaired RER allows fork to travel faster. Moreover, there was an even greater fork distance in the *smc6 rnh201* double mutant (Figure 6D and E), suggesting an additive effect between the two mutations. These data together suggest that the *mph1* and *rnh201* mutations are fundamentally different in their impact on replication fork progression in the *smc6* mutant, thus underscoring the different modes of genetic suppression of *smc6* by these mutations.

We also analysed origin activation in WT versus *smc6* cells by scoring those origins with significant amount of ssDNA in at least two of the three biological replicates in each strain. Our analysis showed that the *smc6* mutant activated more origins than WT (216 versus 157 with 152 in common, Supplementary Figure S3). The 64 *smc6*-specific origins are randomly distributed in the genome and are evenly split between early and late origins (32 in each category). We also

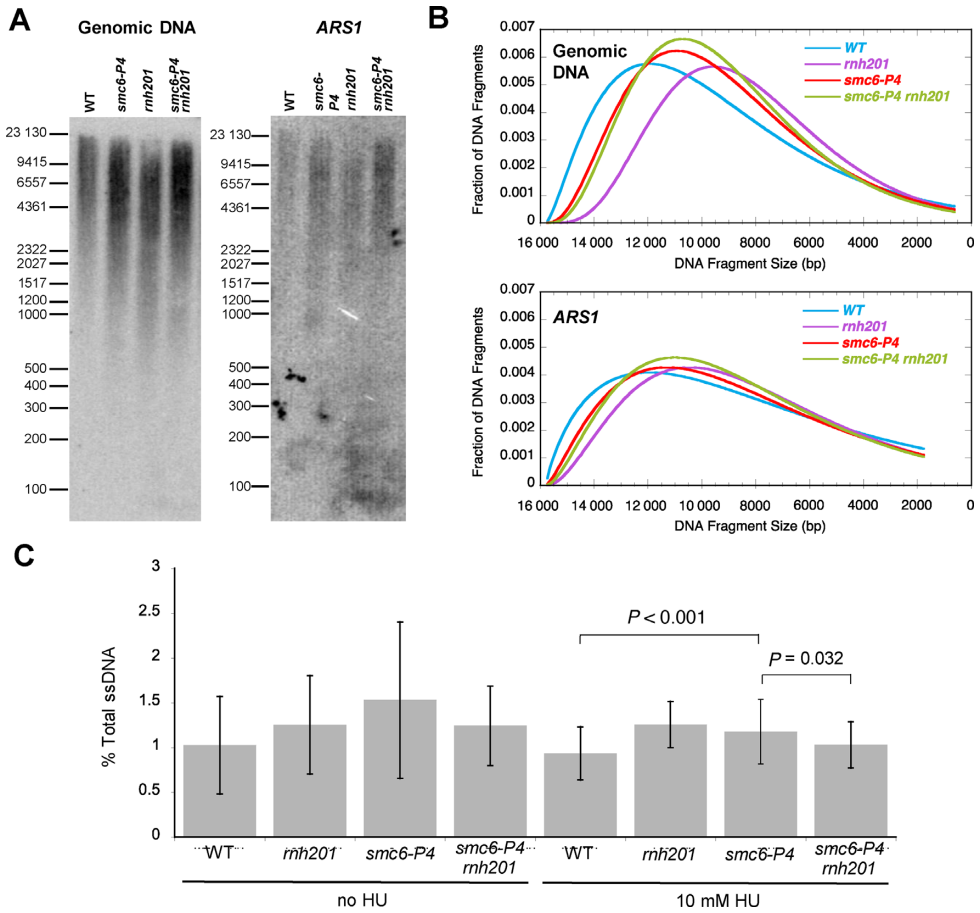

Figure 5. The *smc6-P4* mutant accumulates rNMPs and ssDNA. Genomic DNA isolated from exponentially growing WT, *smc6*, *rnh201Δ* and *smc6 rnh201Δ* cells ($OD_{660} \approx 0.8$) were analyzed for rNMP incorporation by (**A** and **B**) alkaline gel electrophoresis and for percentage of total ssDNA by (**C**) slot blot. (**A**) Autoradiogram of the alkaline gel electrophoresis followed by Southern blotting with either a genomic DNA probe or an *ARS1* probe. Equal amount (4 μg) of DNA was heat-denatured in alkaline buffer and used for alkaline gel electrophoresis, followed by alkaline transfer to nylon membrane and Southern hybridization with a ^{32}P-labelled genomic DNA probe. (**B**) Normalized hybridization signals (using total signals in each sample) in (A) plotted against DNA size. (**C**) Quantification results of total percentage of ssDNA in the genomic DNA by slot blotting un-denatured DNA and hybridization with a genomic DNA probe. Paired Student's *t*-test was performed between WT and *smc6* and between *smc6* and *smc6 rnh201,* and only those relevant comparisons with *P*-values < 0.05 were shown.

show that the vast majority of origins activated in the *smc6* cells are also active in the *smc6 mph1* and *smc6 rnh201* cells, indicating that the *mph1* and *rnh201* mutations have minimal impact on origin activation in the *smc6* mutant (Supplementary Table S4).

Specific blockage of lesion incision in mismatch repair, nucleotide excision repair or base excision repair also suppresses the drug-sensitivity of the *smc6* mutant

Our analysis so far suggests that inhibiting RNase H2 activity in the *smc6* mutant is beneficial during replication stress. We then asked if deletion of genes encoding key components of other repair pathways similarly rescues the drug-sensitivity of *smc6* cells. We tested the removal of Msh2, Msh3 and Msh6 in the mismatch repair (MMR) pathway, Apn1 and Apn2 in the BER pathway, Rad1 and Rad2 in the NER pathway. We observed suppression of *smc6* by all deletions except *apn2Δ*, *msh3Δ* and *rad2Δ* (Supplementary Figure S4). Yeast Apn2 plays a minor role in the incision step of BER with <5% of *in vitro* activity attributed to Apn2 (71), consistent with the observation that *apn2Δ* did not suppress *smc6*. In MMR, the Msh2/Msh6 heterodimer primarily recognizes sites with 1 or 2 nucleotide mismatches, whereas the Msh2/Msh3 dimer is specifically responsible for recognizing a longer (up to 15 nucleotides) mismatched patch due to insertions/deletions (72,73). Therefore, the lack of suppression by *msh3Δ* suggested that the nucleotide mismatches in the *smc6* mutant primarily involve single nucleotides. In the NER pathway, the Rad1–Rad10 complex and Rad2 are structure-dependent endonucleases responsible for the 5′ and 3′ incision of the damaged nucleotide, respectively (74). A study in human cells has suggested that 5′ incision precedes 3′ incision (75). Therefore, *rad1Δ* would preclude Rad2 incision whereas *rad2Δ* would still permit Rad1 incision and thus produce the toxicity in *smc6* cells. Finally, we tested the impact of Exo1, a 5′-3′ exonuclease involved in multiple repair pathways, in mediating damage repair in the *smc6* mutant. We observed only moderate suppression of the HU-sensitivity but not the MMS-sensitivity of the *smc6* mutant (data not shown). This result is not unexpected considering the complicated role of Exo1 in both promot-

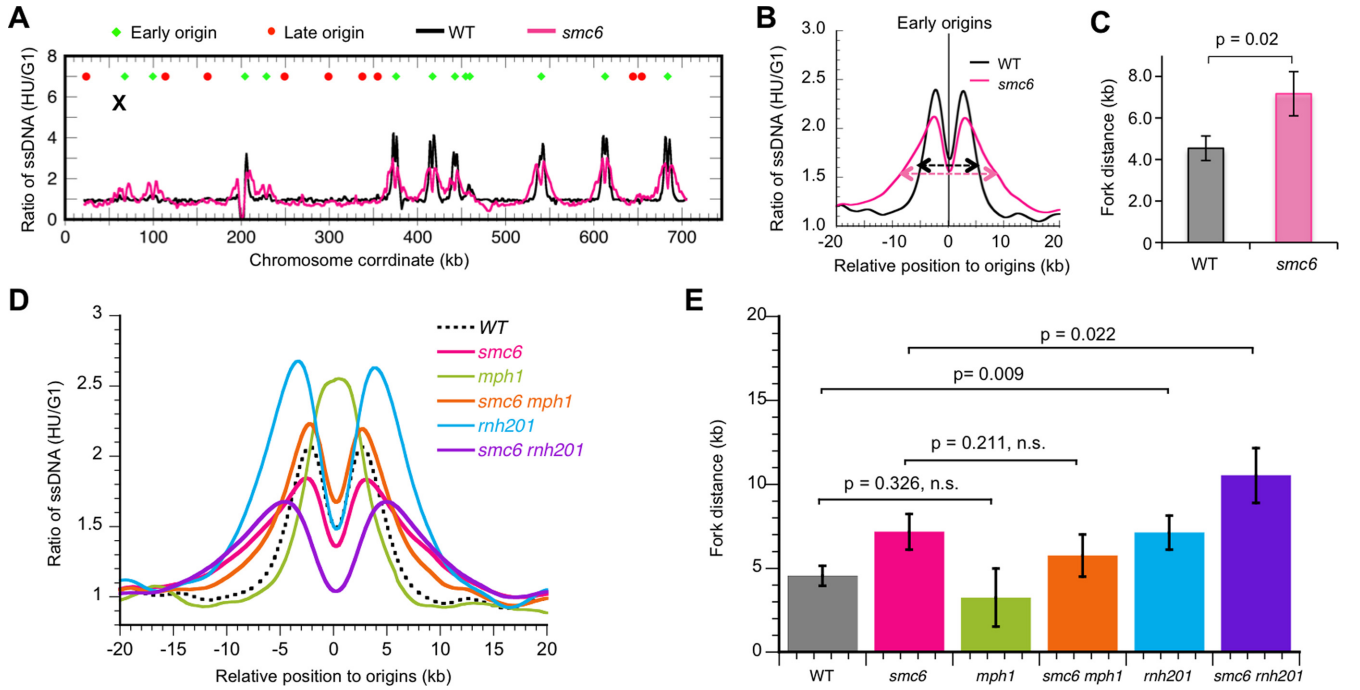

Figure 6. Replication fork progresses faster and ssDNA accumulates behind the replication fork in the *smc6-P4* mutant during acute exposure to HU in S phase. (**A**) Genomic ssDNA mapping in cells synchronously released from α-factor arrest (G1 control sample) into S phase in the presence of 200 mM HU for 1 h (S phase sample). Relative ssDNA enrichment in S phase sample was plotted against chromosome coordinates (kb) for ChrX. Early and late origins are as described in Figure 2. (**B**) Meta-analysis of the ssDNA signals in a 40 kb region encompassing 205 early origins in the *smc6-P4* mutant and WT cells averaged from three independent experiments. (**C**) Distance travelled by replication forks calculated from (B) (see Materials and Methods for detail). (**D**) Comparison between ssDNA formation in the indicated cells using meta-analysis as described in (B). (**E**) Same as in (C), for the indicated strains in (D). Only those relevant comparisons with *P*-values < 0.05 were shown.

ing and interfering with DNA damage repair in different contexts (76,77). In summary, our data taken together also suggest that DNA repair-induced chromosomal DNA processing in the presence of an impaired Smc5/6 complex induces a common detriment to genome stability.

DISCUSSION

The essential function of the Smc5/6 complex during an unperturbed cell cycle has remained enigmatic. By studying genome-wide replication dynamics using density transfer we uncovered evidence for fast-migrating replication forks accompanied by ssDNA formation in the *smc6-P4* mutant, specifically during early S phase. Admittedly subtle and transient as the overall replication dynamics are similar between the *smc6* mutant and WT, this mutant phenotype is consistent with our observation that replication fork-associated DNA traversed a greater distance in the *smc6* mutant than WT during exposure to HU. Thus, our data seem at face value contradictory to a recent study, which demonstrated that precluding Smc5/6 protein expression from S phase does not significantly impact cell viability or S phase progression (42). However, we rationalize that the experimental designs in these two studies are different. First, it is possible that the *smc6-P4* mutation is dominant compared to the depletion of Smc5/6 expression. Second, to examine an unperturbed S phase Menolfi *et al.* relied on EdU-labelling of replicating DNA for 10 to 20 min in an asynchronous population, in contrast to our synchronous release of G1-arrested cells into S phase. Thus, the resolution of early S phase cells in the former was necessarily lower in comparison. Menolfi *et al.* also analysed cells synchronously entering S phase in the presence of HU for 45 or 90 min, compared to the 60 min HU treatment in our experiments. We note that for the 45 min HU-treated sample the BrdU IP-on-chip signals were in fact noticeably wider at the earliest origins (ARS305 and 306) in cells depleted for S phase-specific Smc5/6 than in WT. We also note that longer HU-treatment (such as the 90 min treatment) would likely reduce the difference between replication track lengths. Finally, as conceded above the difference in fork progression between WT and *smc6* cells was rather transient, and therefore would likely elude detection in alternative experimental design. Moreover, our study does not argue against the proposed essential function of the Smc5/6 complex in the G2 phase to resolve recombination structures at genomic sites experiencing endogenous replication stress (42). In fact, in pursuing the cause for the fork migration difference in the *smc6* mutant we found that DNA damage incision is detrimental in the absence of a functional Smc5/6 complex. This discovery provides damage incision during S phase as another reason for the endogenous stress in the *smc6* mutant, in addition to the proposed replication fork pausing-induced stress (42). We also found that *smc6* cells accumulate rNMPs and ssDNA gaps. Therefore, we propose new functions of the Smc5/6 complex in preventing rNMP, and possibly mismatched dNMP, mis-incorporation during replication and ensuring proper DNA repair after

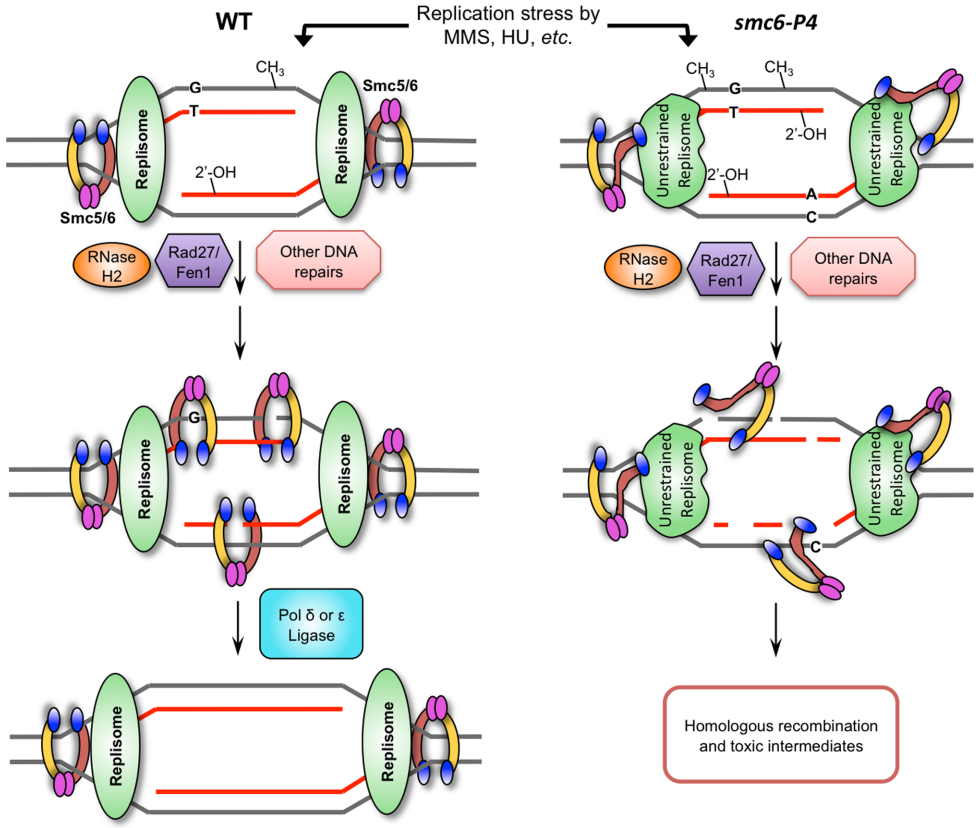

Figure 7. Model of the Smc5/6 complex function during chromosome replication. We propose that the Smc5/6 complex (depicted only as a Smc5/6 heterodimer without the Nse subunits) plays an important function in preventing rNMP and possibly dNMP mis-incorporation. Replication stress-induced replication errors such as rNMP ('2'-OH') and mismatched dNMP ('G-T' or 'A-C' pair) mis-incorporation as well as DNA damage (e.g. methylation, '-CH_3') are properly corrected by multiple repair pathways in the WT cells. But nucleotide incision in the presence of a defective Smc5/6 complex due to the *smc6-P4* mutation leads to extensive ssDNA and formation of toxic HR intermediates. The defective Smc6 protein is depicted as the subunit with a kink. We hypothesize that the *smc6-P4* mutation impairs the ssDNA binding capacity of the Smc5/6 complex, hence the depicted disengagement from the DNA template. However, we note that such a depiction is strictly speculative at this stage. It is unknown if and how Smc5/6 complex interacts with the replisome, or the relative position of the Smc5/6 complex at the replication fork, i.e. whether ahead of or behind the replisome. The authors favour the former possibility as depicted in this model for there are functional interactions between Smc5/6 complex and Topoisomerase II, which serves to relieve torsional stress ahead of the replication fork (41,92).

damage incision (Figure 7). Our model, together with the proposed essential function for the Smc5/6 complex in G2 (42), echoes a previous model where Smc5/6 has multiple functionalities (78).

The genetic suppression of the *smc6-P4* mutant phenotype by virtually all DNA repair pathways was at first surprising because it has been shown that select mutants of the Smc5/6 complex (*nse1*, *mms21* and *smc6-9*), exhibited either no interaction or negative interaction with DNA repair mutants (79,80). Studies in *S. pombe* also reported negative interactions between mutations in the Smc5/6 complex and in DNA repair (13,81–82). We also confirmed that an *mms21Δ* mutant of the Smc5/6 complex is in fact synthetically sick with *rnh201Δ*. In contrast, *rnh201Δ* genetically rescued both *smc6-P4* and *smc6-56*, suggesting that a functional Smc6 subunit is specifically important for coordinating DNA repair during replication stress, possibly through its interaction with and stabilization of ssDNA (see below). Therefore, our analysis underscores the importance of studying allele-specific interactions in order to reveal important functions of the Smc5/6 complex. The genetic suppression of *smc6-P4* by repair mutants is also apparently specific to induced replication stress by HU and MMS. This observation suggests that the DNA damage incision-induced toxicity requires a threshold level of substrates unattainable in the *smc6* mutant without prolonged external replication stress.

Previous studies suggested that *smc6* mutants have elevated mutation and gross chromosomal rearrangement rates (22,23), and here we report that rNMP incorporation is also increased in the mutants. We believe the rNMP substrate in the *smc6* mutant is predominantly single rNMPs incorporated by the processive DNA polymerases, Pol ϵ and Pol δ, rather than those tandem rNMPs synthesized by the Pol α/Primase in the Okazaki fragments. We are led to this conclusion because removal of the RNA primers in Okazaki fragments is performed by RNase H1 (83) and we did not observe genetic suppression by *rnh1Δ* of the *smc6-P4* mutation. We also observed that the introduction of *pol2-M644L* mutation, which incorporates rNMP at a lower level than WT (4,5), into the *smc6* cells led to a reduction of HU sensitivity (data not shown). The genetic

interaction between *smc6* and the MMR pathway suggests the presence of mis-incorporated dNMPs. However, recent studies demonstrated that mismatched rNMPs could also be repaired by the MMR pathway (84,85). Therefore, it is probable that the main substrate for DNA in the *smc6* mutant is mismatched rNMPs, instead of dNMPs. We also observed evidence for BER and NER substrates in the *smc6* mutant during replication stress, presumably due to the alkylation damage produced by MMS as well as base oxidation during oxidative stress known to occur in both HU and MMS treatment (86).

We also propose that DNA damage incision in the presence of a defective Smc5/6 complex generates toxic intermediates due to extensive ssDNA formation and subsequent engagement in HR. Our analysis did not reveal negative genetic interaction between *smc6-P4* with either *hnt3Δ* or *top1Δ,* arguing against 5′-adenylated rNMP or 2′-3′ cyclic phosphate, respectively, being the toxic intermediate precipitating cell death. Therefore, the simplest explanation for the increased density of replicated DNA and toxicity associated with nucleotide incision by multiple nucleases in the *smc6* mutant is persistent ssDNA formation. The *smc6* mutant might be defective in short patch synthesis by Pol δ and/or subsequent ligation by DNA ligase I, leaving a ssDNA gap in the template DNA. However, a gap of single nucleotide is unlikely responsible for the density change of the duplex DNA. Therefore, the persistent single nucleotide gap in the *smc6* mutant might be converted to a longer patch of ssDNA to initiate HR.

Our study thus points to a novel role of the Smc5/6 complex, i.e. in preventing unsupervised ssDNA formation during DNA replication as a result of damage incision. Defects in this pathway then manifest in unresolved HR intermediates and sister chromatids non-disjunction. Both Smc5p and Smc6p have two independent DNA binding regions, one near the hinge domain and the other one near the ATPase domain. The *smc6-P4* (K239R) mutation resides very close to the ATPase domain and therefore likely impacts DNA binding of the Smc6 protein. Indeed, Smc5p, Smc6p and the heterodimer all have higher binding affinity towards ssDNA than dsDNA (87–89). Moreover, the ssDNA affinity is even higher than Rad51p (90,91). Therefore, we speculate that the Smc5/6 complex is instrumental in binding and stabilizing ssDNA arising from multiple DNA repair processes, thus protecting them from being engaged in pathological homologous recombination events.

Finally, during our investigation we also revealed intriguing phenotypes of replication fork progression in the *mph1Δ* and *rnh201Δ* mutants in HU. First, replication forks appeared to traverse further in the absence of RNase H2, suggesting that inactivating the RER pathway accelerates fork speed. We also note that the *mph1Δ* mutant did not show the 'split peak' ssDNA signals as did other strains (Figure 6D). It is unclear whether this phenotype is due to unresolved bi-directional forks (limited by the resolution of the microarray) or elevated level of ssDNA *behind* the replication forks as opposed to *at* the forks. We favour the latter possibility because WT cells, with similar fork progression, showed well-resolved bi-directional forks. It will be interesting to further dissect the ssDNA species at versus behind replication forks in these cells with the advent of higher resolution methods in the future.

SUPPLEMENTARY DATA

Supplementary Data are available at NAR Online.

ACKNOWLEDGEMENT

The authors wish to thank X. Zhao for providing yeast strains and significant intellectual contributions; S. Lujan and J. Williams for generous help with alkaline gel electrophoresis data analysis; A. McCulley and B. Haarer for technical support; D. Amberg, S. Loh and S. Hanes for sharing equipment; D. Amberg, L. Symington and T. Kunkel for yeast strains and plasmids; and M. K. Raghuraman and X-J. Chen for critically reading the manuscript. We also thank the Feng lab members for general support and helpful discussions.

FUNDING

National Institutes of Health (NIH) [4R00GM08137804 to W.F.]; Upstate Medical University [to W. F]. Funding for open access charge: Institutional funds from SUNY Upstate Medical University.
Conflict of interest statement. None declared.

REFERENCES

1. Raghuraman,M.K., Winzeler,E.A., Collingwood,D., Hunt,S., Wodicka,L., Conway,A., Lockhart,D.J., Davis,R.W., Brewer,B.J. and Fangman,W.L. (2001) Replication dynamics of the yeast genome. *Science*, **294**, 115–121.
2. Alvino,G.M., Collingwood,D., Murphy,J.M., Delrow,J., Brewer,B.J. and Raghuraman,M.K. (2007) Replication in hydroxyurea: It's a matter of time. *Mol. Cell. Biol.*, **27**, 6396–6406.
3. Joyce,C.M. (1997) Choosing the right sugar: how polymerases select a nucleotide substrate. *Proc. Natl. Acad. Sci. U.S.A.*, **94**, 1619–1622.
4. Nick McElhinny,S.A., Kumar,D., Clark,A.B., Watt,D.L., Watts,B.E., Lundstrom,E.B., Johansson,E., Chabes,A. and Kunkel,T.A. (2010) Genome instability due to ribonucleotide incorporation into DNA. *Nat. Chem. Biol.*, **6**, 774–781.
5. Nick McElhinny,S.A., Watts,B.E., Kumar,D., Watt,D.L., Lundstrom,E.B., Burgers,P.M., Johansson,E., Chabes,A. and Kunkel,T.A. (2010) Abundant ribonucleotide incorporation into DNA by yeast replicative polymerases. *Proc. Natl. Acad. Sci. U.S.A.*, **107**, 4949–4954.
6. Kunkel,T.A. (2011) Balancing eukaryotic replication asymmetry with replication fidelity. *Curr. Opin. Chem. Biol.*, **15**, 620–626.
7. Boiteux,S. and Jinks-Robertson,S. (2013) DNA repair mechanisms and the bypass of DNA damage in Saccharomyces cerevisiae. *Genetics*, **193**, 1025–1064.
8. Fujioka,Y., Kimata,Y., Nomaguchi,K., Watanabe,K. and Kohno,K. (2002) Identification of a novel non-structural maintenance of chromosomes (SMC) component of the SMC5-SMC6 complex involved in DNA repair. *J. Biol. Chem.*, **277**, 21585–21591.
9. McDonald,W.H., Pavlova,Y., Yates,J.R. 3rd and Boddy,M.N. (2003) Novel essential DNA repair proteins Nse1 and Nse2 are subunits of the fission yeast Smc5-Smc6 complex. *J. Biol. Chem.*, **278**, 45460–45467.
10. Pebernard,S., McDonald,W.H., Pavlova,Y., Yates,J.R. 3rd and Boddy,M.N. (2004) Nse1, Nse2, and a novel subunit of the Smc5-Smc6 complex, Nse3, play a crucial role in meiosis. *Mol. Biol. Cell*, **15**, 4866–4876.
11. Sergeant,J., Taylor,E., Palecek,J., Fousteri,M., Andrews,E.A., Sweeney,S., Shinagawa,H., Watts,F.Z. and Lehmann,A.R. (2005) Composition and architecture of the Schizosaccharomyces pombe Rad18 (Smc5-6) complex. *Mol. Cell. Biol.*, **25**, 172–184.

12. Andrews,E.A., Palecek,J., Sergeant,J., Taylor,E., Lehmann,A.R. and Watts,F.Z. (2005) Nse2, a component of the Smc5-6 complex, is a SUMO ligase required for the response to DNA damage. *Mol. Cell. Biol.*, **25**, 185–196.
13. Morikawa,H., Morishita,T., Kawane,S., Iwasaki,H., Carr,A.M. and Shinagawa,H. (2004) Rad62 protein functionally and physically associates with the smc5/smc6 protein complex and is required for chromosome integrity and recombination repair in fission yeast. *Mol. Cell. Biol.*, **24**, 9401–9413.
14. Pebernard,S., Wohlschlegel,J., McDonald,W.H., Yates,J.R. 3rd and Boddy,M.N. (2006) The Nse5-Nse6 dimer mediates DNA repair roles of the Smc5-Smc6 complex. *Mol. Cell. Biol.*, **26**, 1617–1630.
15. Zhao,X. and Blobel,G. (2005) A SUMO ligase is part of a nuclear multiprotein complex that affects DNA repair and chromosomal organization. *Proc. Natl. Acad. Sci. U.S.A.*, **102**, 4777–4782.
16. Verkade,H.M., Bugg,S.J., Lindsay,H.D., Carr,A.M. and O'Connell,M.J. (1999) Rad18 is required for DNA repair and checkpoint responses in fission yeast. *Mol. Biol. Cell*, **10**, 2905–2918.
17. Lehmann,A.R. (1996) Molecular biology of DNA repair in the fission yeast Schizosaccharomyces pombe. *Mutat. Res.*, **363**, 147–161.
18. Koshland,D. and Strunnikov,A. (1996) Mitotic chromosome condensation. *Annu. Rev. Dev. Biol.*, **12**, 305–333.
19. De Piccoli,G., Torres-Rosell,J. and Aragon,L. (2009) The unnamed complex: What do we know about Smc5-Smc6? *Chromosome Res.*, **17**, 251–263.
20. Fousteri,M.I. and Lehmann,A.R. (2000) A novel SMC protein complex in Schizosaccharomyces pombe contains the Rad18 DNA repair protein. *EMBO J.*, **19**, 1691–1702.
21. Ampatzidou,E., Irmisch,A., O'Connell,M.J. and Murray,J.M. (2006) Smc5/6 is required for repair at collapsed replication forks. *Mol. Cell. Biol.*, **26**, 9387–9401.
22. De Piccoli,G., Cortes-Ledesma,F., Ira,G., Torres-Rosell,J., Uhle,S., Farmer,S., Hwang,J.Y., Machin,F., Ceschia,A., McAleenan,A. *et al.* (2006) Smc5-Smc6 mediate DNA double-strand-break repair by promoting sister-chromatid recombination. *Nat. Cell Biol.*, **8**, 1032–1034.
23. Hwang,J.Y., Smith,S., Ceschia,A., Torres-Rosell,J., Aragon,L. and Myung,K. (2008) Smc5-Smc6 complex suppresses gross chromosomal rearrangements mediated by break-induced replications. *DNA Repair (Amst)*, **7**, 1426–1436.
24. Chen,Y.H., Choi,K., Szakal,B., Arenz,J., Duan,X., Ye,H., Branzei,D. and Zhao,X. (2009) Interplay between the Smc5/6 complex and the Mph1 helicase in recombinational repair. *Proc. Natl. Acad. Sci. U.S.A.*, **106**, 21252–21257.
25. Kliszczak,M., Stephan,A.K., Flanagan,A.M. and Morrison,C.G. (2012) SUMO ligase activity of vertebrate Mms21/Nse2 is required for efficient DNA repair but not for Smc5/6 complex stability. *DNA Repair (Amst)*, **11**, 799–810.
26. Tapia-Alveal,C. and O'Connell,M.J. (2011) Nse1-dependent recruitment of Smc5/6 to lesion-containing loci contributes to the repair defects of mutant complexes. *Mol. Biol. Cell*, **22**, 4669–4682.
27. Stephan,A.K., Kliszczak,M. and Morrison,C.G. (2011) The Nse2/Mms21 SUMO ligase of the Smc5/6 complex in the maintenance of genome stability. *FEBS Lett.*, **585**, 2907–2913.
28. Chiolo,I., Minoda,A., Colmenares,S.U., Polyzos,A., Costes,S.V. and Karpen,G.H. (2011) Double-strand breaks in heterochromatin move outside of a dynamic HP1a domain to complete recombinational repair. *Cell*, **144**, 732–744.
29. Choi,K., Szakal,B., Chen,Y.H., Branzei,D. and Zhao,X. (2010) The Smc5/6 complex and Esc2 influence multiple replication-associated recombination processes in Saccharomyces cerevisiae. *Mol. Biol. Cell*, **21**, 2306–2314.
30. Chen,Y.H., Szakal,B., Castellucci,F., Branzei,D. and Zhao,X. (2013) DNA damage checkpoint and recombinational repair differentially affect the replication stress tolerance of Smc6 mutants. *Mol. Biol. Cell*, **24**, 2431–2441.
31. Torres-Rosell,J., Machin,F., Farmer,S., Jarmuz,A., Eydmann,T., Dalgaard,J.Z. and Aragon,L. (2005) SMC5 and SMC6 genes are required for the segregation of repetitive chromosome regions. *Nat. Cell Biol.*, **7**, 412–419.
32. Gallego-Paez,L.M., Tanaka,H., Bando,M., Takahashi,M., Nozaki,N., Nakato,R., Shirahige,K. and Hirota,T. (2014) Smc5/6-mediated regulation of replication progression contributes to chromosome assembly during mitosis in human cells. *Mol. Biol. Cell*, **25**, 302–317.
33. Lindroos,H.B., Strom,L., Itoh,T., Katou,Y., Shirahige,K. and Sjogren,C. (2006) Chromosomal association of the Smc5/6 complex reveals that it functions in differently regulated pathways. *Mol. Cell*, **22**, 755–767.
34. Xaver,M., Huang,L., Chen,D. and Klein,F. (2013) Smc5/6-Mms21 prevents and eliminates inappropriate recombination intermediates in meiosis. *PLoS Genet.*, **9**, e1004067.
35. Copsey,A., Tang,S., Jordan,P.W., Blitzblau,H.G., Newcombe,S., Chan,A.C., Newnham,L., Li,Z., Gray,S., Herbert,A.D. *et al.* (2013) Smc5/6 coordinates formation and resolution of joint molecules with chromosome morphology to ensure meiotic divisions. *PLoS Genet.*, **9**, e1004071.
36. Xue,X., Choi,K., Bonner,J., Chiba,T., Kwon,Y., Xu,Y., Sanchez,H., Wyman,C., Niu,H., Zhao,X. *et al.* (2014) Restriction of replication fork regression activities by a conserved SMC complex. *Mol. Cell*, **56**, 436–445.
37. Cho,R.J., Campbell,M.J., Winzeler,E.A., Steinmetz,L., Conway,A., Wodicka,L., Wolfsberg,T.G., Gabrielian,A.E., Landsman,D., Lockhart,D.J. *et al.* (1998) A genome-wide transcriptional analysis of the mitotic cell cycle. *Mol. Cell*, **2**, 65–73.
38. Spellman,P.T., Sherlock,G., Zhang,M.Q., Iyer,V.R., Anders,K., Eisen,M.B., Brown,P.O., Botstein,D. and Futcher,B. (1998) Comprehensive identification of cell cycle-regulated genes of the yeast Saccharomyces cerevisiae by microarray hybridization. *Mol. Biol. Cell*, **9**, 3273–3297.
39. Germann,S.M., Schramke,V., Pedersen,R.T., Gallina,I., Eckert-Boulet,N., Oestergaard,V.H. and Lisby,M. (2014) TopBP1/Dpb11 binds DNA anaphase bridges to prevent genome instability. *J. Cell Biol.*, **204**, 45–59.
40. Torres-Rosell,J., De Piccoli,G., Cordon-Preciado,V., Farmer,S., Jarmuz,A., Machin,F., Pasero,P., Lisby,M., Haber,J.E. and Aragon,L. (2007) Anaphase onset before complete DNA replication with intact checkpoint responses. *Science*, **315**, 1411–1415.
41. Kegel,A., Betts-Lindroos,H., Kanno,T., Jeppsson,K., Strom,L., Katou,Y., Itoh,T., Shirahige,K. and Sjogren,C. (2011) Chromosome length influences replication-induced topological stress. *Nature*, **471**, 392–396.
42. Menolfi,D., Delamarre,A., Lengronne,A., Pasero,P. and Branzei,D. (2015) Essential roles of the Smc5/6 complex in replication through natural pausing sites and endogenous DNA damage tolerance. *Mol. Cell*, **60**, 835–846.
43. Thomas,B.J. and Rothstein,R. (1989) Elevated recombination rates in transcriptionally active DNA. *Cell*, **56**, 619–630.
44. Entian,K.D., Schuster,T., Hegemann,J.H., Becher,D., Feldmann,H., Guldener,U., Gotz,R., Hansen,M., Hollenberg,C.P., Jansen,G. *et al.* (1999) Functional analysis of 150 deletion mutants in Saccharomyces cerevisiae by a systematic approach. *Mol. Gen. Genet.*, **262**, 683–702.
45. Pavlov,Y.I., Shcherbakova,P.V. and Kunkel,T.A. (2001) In vivo consequences of putative active site mutations in yeast DNA polymerases alpha, epsilon, delta, and zeta. *Genetics*, **159**, 47–64.
46. Peng,J., Raghuraman,M.K. and Feng,W. (2014) Analysis of replication timing using synchronized budding yeast cultures. *Methods Mol. Biol.*, **1170**, 477–499.
47. Feng,W., Collingwood,D., Boeck,M.E., Fox,L.A., Alvino,G.M., Fangman,W.L., Raghuraman,M.K. and Brewer,B.J. (2006) Genomic mapping of single-stranded DNA in hydroxyurea-challenged yeasts identifies origins of replication. *Nat. Cell Biol.*, **8**, 148–155.
48. Peng,J., Raghuraman,M.K. and Feng,W. (2014) Analysis of ssDNA gaps and DSBs in genetically unstable yeast cultures. *Methods Mol. Biol.*, **1170**, 501–515.
49. Hang,L.E., Peng,J., Tan,W., Szakal,B., Menolfi,D., Sheng,Z., Lobachev,K., Branzei,D., Feng,W. and Zhao,X. (2015) Rtt107 Is a multi-functional scaffold supporting replication progression with partner SUMO and ubiquitin ligases. *Mol. Cell*, **60**, 268–279.
50. Wells,R.D. and Larson,J.E. (1972) Buoyant density studies on natural and synthetic deoxyribonucleic acids in neutral and alkaline solutions. *J. Biol. Chem.*, **247**, 3405–3409.
51. Taylor,J.H., Wu,M., Erickson,L.C. and Kurek,M.P. (1975) Replication of DNA in mammalian chromosomes. III. Size and RNA content of Okazaki fragments. *Chromosoma*, **53**, 175–189.

52. Rydberg,B. and Game,J. (2002) Excision of misincorporated ribonucleotides in DNA by RNase H (type 2) and FEN-1 in cell-free extracts. *Proc. Natl. Acad. Sci. U.S.A.*, **99**, 16654–16659.
53. Kim,N., Huang,S.N., Williams,J.S., Li,Y.C., Clark,A.B., Cho,J.E., Kunkel,T.A., Pommier,Y. and Jinks-Robertson,S. (2011) Mutagenic processing of ribonucleotides in DNA by yeast topoisomerase I. *Science*, **332**, 1561–1564.
54. Jeong,H.S., Backlund,P.S., Chen,H.C., Karavanov,A.A. and Crouch,R.J. (2004) RNase H2 of Saccharomyces cerevisiae is a complex of three proteins. *Nucleic Acids Res.*, **32**, 407–414.
55. Eder,P.S., Walder,R.Y. and Walder,J.A. (1993) Substrate specificity of human RNase H1 and its role in excision repair of ribose residues misincorporated in DNA. *Biochimie*, **75**, 123–126.
56. Chon,H., Sparks,J.L., Rychlik,M., Nowotny,M., Burgers,P.M., Crouch,R.J. and Cerritelli,S.M. (2013) RNase H2 roles in genome integrity revealed by unlinking its activities. *Nucleic Acids Res.*, **41**, 3130–3143.
57. Allen-Soltero,S., Martinez,S.L., Putnam,C.D. and Kolodner,R.D. (2014) A saccharomyces cerevisiae RNase H2 interaction network functions to suppress genome instability. *Mol. Cell. Biol.*, **34**, 1521–1534.
58. Hegnauer,A.M., Hustedt,N., Shimada,K., Pike,B.L., Vogel,M., Amsler,P., Rubin,S.M., van Leeuwen,F., Guenole,A., van Attikum,H. *et al.* (2012) An N-terminal acidic region of Sgs1 interacts with Rpa70 and recruits Rad53 kinase to stalled forks. *EMBO J.*, **31**, 3768–3783.
59. Ii,M. and Brill,S.J. (2005) Roles of SGS1, MUS81, and RAD51 in the repair of lagging-strand replication defects in Saccharomyces cerevisiae. *Curr. Genet.*, **48**, 213–225.
60. Torres-Rosell,J., Sunjevaric,I., De Piccoli,G., Sacher,M., Eckert-Boulet,N., Reid,R., Jentsch,S., Rothstein,R., Aragon,L. and Lisby,M. (2007) The Smc5-Smc6 complex and SUMO modification of Rad52 regulates recombinational repair at the ribosomal gene locus. *Nat. Cell Biol.*, **9**, 923–931.
61. Leung,G.P., Lee,L., Schmidt,T.I., Shirahige,K. and Kobor,M.S. (2011) Rtt107 is required for recruitment of the SMC5/6 complex to DNA double strand breaks. *J. Biol. Chem.*, **286**, 26250–26257.
62. Prakash,L. and Prakash,S. (1977) Isolation and characterization of MMS-sensitive mutants of Saccharomyces cerevisiae. *Genetics*, **86**, 33–55.
63. Prakash,S. and Prakash,L. (1977) Increased spontaneous mitotic segregation in MMS-sensitive mutants of Saccharomyces cerevisiae. *Genetics*, **87**, 229–236.
64. Clausen,A.R., Williams,J.S. and Kunkel,T.A. (2015) Measuring ribonucleotide incorporation into DNA in vitro and in vivo. *Methods Mol. Biol.*, **1300**, 123–139.
65. Garvik,B., Carson,M. and Hartwell,L. (1995) Single-stranded DNA arising at telomeres in cdc13 mutants may constitute a specific signal for the RAD9 checkpoint. *Mol. Cell. Biol.*, **15**, 6128–6138.
66. Tumbale,P., Williams,J.S., Schellenberg,M.J., Kunkel,T.A. and Williams,R.S. (2014) Aprataxin resolves adenylated RNA-DNA junctions to maintain genome integrity. *Nature*, **506**, 111–115.
67. Sekiguchi,J. and Shuman,S. (1997) Site-specific ribonuclease activity of eukaryotic DNA topoisomerase I. *Mol. Cell*, **1**, 89–97.
68. Williams,J.S., Smith,D.J., Marjavaara,L., Lujan,S.A., Chabes,A. and Kunkel,T.A. (2013) Topoisomerase 1-mediated removal of ribonucleotides from nascent leading-strand DNA. *Mol. Cell*, **49**, 1010–1015.
69. Ahel,I., Rass,U., El-Khamisy,S.F., Katyal,S., Clements,P.M., McKinnon,P.J., Caldecott,K.W. and West,S.C. (2006) The neurodegenerative disease protein aprataxin resolves abortive DNA ligation intermediates. *Nature*, **443**, 713–716.
70. Bustard,D.E., Menolfi,D., Jeppsson,K., Ball,L.G., Dewey,S.C., Shirahige,K., Sjogren,C., Branzei,D. and Cobb,J.A. (2012) During replication stress, non-SMC element 5 (NSE5) is required for Smc5/6 protein complex functionality at stalled forks. *J. Biol. Chem.*, **287**, 11374–11383.
71. Popoff,S.C., Spira,A.I., Johnson,A.W. and Demple,B. (1990) Yeast structural gene (APN1) for the major apurinic endonuclease: homology to Escherichia coli endonuclease IV. *Proc. Natl. Acad. Sci. U.S.A.*, **87**, 4193–4197.
72. Harrington,J.M. and Kolodner,R.D. (2007) Saccharomyces cerevisiae Msh2-Msh3 acts in repair of base-base mispairs. *Mol. Cell. Biol.*, **27**, 6546–6554.
73. Kunkel,T.A. and Erie,D.A. (2005) DNA mismatch repair. *Annu. Rev. Biochem.*, **74**, 681–710.
74. Evans,E., Moggs,J.G., Hwang,J.R., Egly,J.M. and Wood,R.D. (1997) Mechanism of open complex and dual incision formation by human nucleotide excision repair factors. *EMBO J.*, **16**, 6559–6573.
75. Staresincic,L., Fagbemi,A.F., Enzlin,J.H., Gourdin,A.M., Wijgers,N., Dunand-Sauthier,I., Giglia-Mari,G., Clarkson,S.G., Vermeulen,W. and Scharer,O.D. (2009) Coordination of dual incision and repair synthesis in human nucleotide excision repair. *EMBO J.*, **28**, 1111–1120.
76. Giannattasio,M., Follonier,C., Tourriere,H., Puddu,F., Lazzaro,F., Pasero,P., Lopes,M., Plevani,P. and Muzi-Falconi,M. (2010) Exo1 competes with repair synthesis, converts NER intermediates to long ssDNA gaps, and promotes checkpoint activation. *Mol. Cell*, **40**, 50–62.
77. Sparks,J.L., Chon,H., Cerritelli,S.M., Kunkel,T.A., Johansson,E., Crouch,R.J. and Burgers,P.M. (2012) RNase H2-initiated ribonucleotide excision repair. *Mol. Cell*, **47**, 980–986.
78. Irmisch,A., Ampatzidou,E., Mizuno,K., O'Connell,M.J. and Murray,J.M. (2009) Smc5/6 maintains stalled replication forks in a recombination-competent conformation. *EMBO J.*, **28**, 144–155.
79. Chavez,A., Agrawal,V. and Johnson,F.B. (2011) Homologous recombination-dependent rescue of deficiency in the structural maintenance of chromosomes (Smc) 5/6 complex. *J. Biol. Chem.*, **286**, 5119–5125.
80. Santa Maria,S.R., Gangavarapu,V., Johnson,R.E., Prakash,L. and Prakash,S. (2007) Requirement of Nse1, a subunit of the Smc5-Smc6 complex, for Rad52-dependent postreplication repair of UV-damaged DNA in Saccharomyces cerevisiae. *Mol. Cell. Biol.*, **27**, 8409–8418.
81. Lee,K.M., Nizza,S., Hayes,T., Bass,K.L., Irmisch,A., Murray,J.M. and O'Connell,M.J. (2007) Brc1-mediated rescue of Smc5/6 deficiency: requirement for multiple nucleases and a novel Rad18 function. *Genetics*, **175**, 1585–1595.
82. Sheedy,D.M., Dimitrova,D., Rankin,J.K., Bass,K.L., Lee,K.M., Tapia-Alveal,C., Harvey,S.H., Murray,J.M. and O'Connell,M.J. (2005) Brc1-mediated DNA repair and damage tolerance. *Genetics*, **171**, 457–468.
83. Huang,L., Kim,Y., Turchi,J.J. and Bambara,R.A. (1994) Structure-specific cleavage of the RNA primer from Okazaki fragments by calf thymus RNase HI. *J. Biol. Chem.*, **269**, 25922–25927.
84. Ghodgaonkar,M.M., Lazzaro,F., Olivera-Pimentel,M., Artola-Boran,M., Cejka,P., Reijns,M.A., Jackson,A.P., Plevani,P., Muzi-Falconi,M. and Jiricny,J. (2013) Ribonucleotides misincorporated into DNA act as strand-discrimination signals in eukaryotic mismatch repair. *Mol. Cell*, **50**, 323–332.
85. Shen,Y., Koh,K.D., Weiss,B. and Storici,F. (2012) Mispaired rNMPs in DNA are mutagenic and are targets of mismatch repair and RNases H. *Nat. Struct. Mol. Biol.*, **19**, 98–104.
86. Travesa,A., Kuo,D., de Bruin,R.A., Kalashnikova,T.I., Guaderrama,M., Thai,K., Aslanian,A., Smolka,M.B., Yates,J.R. 3rd, Ideker,T. *et al.* (2012) DNA replication stress differentially regulates G1/S genes via Rad53-dependent inactivation of Nrm1. *EMBO J.*, **31**, 1811–1822.
87. Roy,M.A. and D'Amours,D. (2011) DNA-binding properties of Smc6, a core component of the Smc5-6 DNA repair complex. *Biochem. Biophys. Res. Commun.*, **416**, 80–85.
88. Roy,M.A., Siddiqui,N. and D'Amours,D. (2011) Dynamic and selective DNA-binding activity of Smc5, a core component of the Smc5-Smc6 complex. *Cell Cycle*, **10**, 690–700.
89. Roy,M.A., Dhanaraman,T. and D'Amours,D. (2015) The Smc5-Smc6 heterodimer associates with DNA through several independent binding domains. *Sci. Rep.*, **5**, 9797.
90. Cloud,V., Chan,Y.L., Grubb,J., Budke,B. and Bishop,D.K. (2012) Rad51 is an accessory factor for Dmc1-mediated joint molecule formation during meiosis. *Science*, **337**, 1222–1225.
91. Zaitseva,E.M., Zaitsev,E.N. and Kowalczykowski,S.C. (1999) The DNA binding properties of Saccharomyces cerevisiae Rad51 protein. *J. Biol. Chem.*, **274**, 2907–2915.
92. Tapia-Alveal,C., Outwin,E.A., Trempolec,N., Dziadkowiec,D., Murray,J.M. and O'Connell,M.J. (2010) SMC complexes and topoisomerase II work together so that sister chromatids can work apart. *Cell Cycle*, **9**, 2065–2070.